Zentrum für Technomathematik
Fachbereich 3 – Mathematik und Informatik

FINITE ELEMENT SIMULATION OF A MATERIAL ACCUMULATION PROCESS INCLUDING PHASE TRANSITIONS AND A CAPILLARY SURFACE

Mischa Jahn **Alfred Schmidt**

Report 12-03

Berichte aus der Technomathematik

Report 12-03 November 2012

FINITE ELEMENT SIMULATION OF A MATERIAL ACCUMULATION PROCESS INCLUDING PHASE TRANSITIONS AND A CAPILLARY SURFACE

M. JAHN AND A. SCHMIDT

Abstract. In this article, the modeling and simulation of a material accumulation process in micro-range based on laser-based free form heading is discussed. The process represents the first step of a material accumulation process which has been developed within the SFB 747 and is modeled mathematically by coupling the Stefan problem with the Navier-Stokes equations including a free capillary surface. For the numerical simulation of the process, two different approaches for handling solid-liquid phase transitions are combined and implemented in a finite element method.

1. Introduction

In modern production engineering, the need for smaller components and more process efficiency is of growing interest. Unfortunately, with increasing miniaturization, methods used in macro-scale are sometimes no longer applicable to very small work-pieces, making the production of micro-components a challenging task. A characteristic example for a process in which problems arises due to miniaturization is a forming process for metallic micro-components.

Conventionally, a multilevel cold forming approach is applied to the work-piece in macro-scale, in order to accumulate a certain length l_0 of a sample with diameter d_0 and forming it simultaneously. Unfortunately, the upset ratio $s := \frac{l_0}{d_0}$ achievable by these methods is very limited and decreases if d_0 does.

Therefore, the Collaborative Research Center 747 "Micro Cold Forming" developed a two-level cold forming process for metallic components in micro-range. The first step of the process is laser-based free form heading [11, 16, 20] which takes advantage of size effects [18, 19]. In detail, the ratio of surface area of the melt to its volume causes surface tension dominating gravity, forming the melt to an almost perfect sphere. After solidification, the generated spherical material accumulation can be formed in a secondary step of the process.

By using a laser, energy can be applied very precisely (regarding space and time) to the work-piece making the process very efficient. Furthermore, the forming properties of the material accumulation generated by laser-based free form heading are very good. A visualization of a conventional cold forming process and the two-level cold forming process is given in Figure 1.1.

The material accumulation process can be modeled mathematically by coupling the Stefan problem for taking phase transitions into account with the Navier-Stokes equations including a free capillary surface for describing the dynamics in the melt. Both, the Stefan problem and the Navier-Stokes equations with a capillary surface have a long history in pure and applied mathematics and have been discussed in many publications, e.g. [2, 4, 8, 13, 17]. However, coupling both problems has been discussed much less, e.g. [5–7], and is still challenging due to the interdependence of geometry and solid-liquid-interface. In this paper, the approach for handling

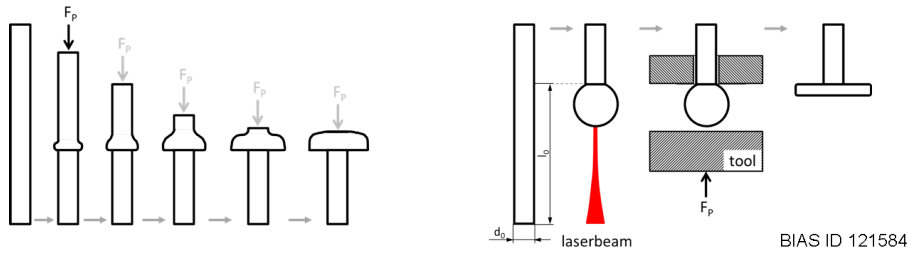

FIGURE 1.1. Conventional multilevel cold forming process (left) and two-level cold forming process used by SFB 747 (right)

this interdependence bases on the combination of a enthalpy model [8] and a sharp interface model [6] which has been first presented in [10].

2. Mathematical model

The model of the melting and solidification process includes the energy balance depending on laser heating, heat transport, radiation described by the Stefan-Boltzmann law, forced convection and phase transitions. Additionally, the dynamics in the melt and its free capillary surface are considered.

Before describing the model, we make some assumptions to simplify matters: Firstly, we use constant material parameters for each subdomain, indicated by the index l for liquid and s for solid. Vaporization effects are neglected and we assume the melt to be incompressible so we can use the incompressible Navier-Stokes equations. Furthermore, the buoyancy effects are modeled by the Boussinesq approximation.

2.1. Continuum model.

Let $\Omega(t) = \Omega_s(t) \cup \Omega_l(t) \cup \Gamma_S(t) \subset \mathbb{R}^3$ be the time dependent domain for $t \in [t_0, t_f]$, consisting of a solid subdomain $\Omega_s(t)$, a liquid subdomain $\Omega_l(t)$ and a solid-liquid interface $\Gamma_S(t)$. The domain boundary $\partial\Omega(t) = \Gamma_C(t) \cup \Gamma_R(t) \cup \Gamma_N(t)$ with disjoint sets $\Gamma_C(t)$, $\Gamma_R(t)$ and $\Gamma_N(t)$, is distinguished in parts with different boundary conditions. Here, $\Gamma_C(t)$ denotes the free capillary surface of the melt. A sketch of the different domains and their boundaries is given in Figure 2.1. Initially, we have $\Omega_l(0) = \emptyset$, $\Gamma_S(0) = \emptyset$ and $\partial\Omega(0) = \Gamma_R(t) \cup \Gamma_N(t)$.

The process is modeled by the Stefan problem in the whole domain for the temperature $T\colon \Omega(t) \to \mathbb{R}$ which is coupled with the incompressible Navier-Stokes equations in the melt $\Omega_l(t)$ with a capillary surface for the velocity field of the fluid $u\colon \Omega_l(t) \to \mathbb{R}^3$ and its pressure $p\colon \Omega_l(t) \to \mathbb{R}$.

In non-dimensional units, the model given by the PDE-system

$$\partial_t u + u \cdot \nabla u - \nabla \cdot \left(\frac{1}{\mathrm{Re}} \mathrm{D}(u) - p \mathrm{I_d} \right) = -\frac{\mathrm{Bo}}{\mathrm{We}} e_2 + \frac{\mathrm{Gr}}{\mathrm{Re}^2} T e_2 \qquad \text{in } \Omega_l(t), \tag{2.1}$$

$$\nabla \cdot u = 0 \qquad \text{in } \Omega_l(t), \tag{2.2}$$

$$\partial_t T + u \cdot \nabla T - \frac{1}{\mathrm{RePr}} \Delta T = 0 \qquad \text{in } \Omega_l(t), \tag{2.3}$$

$$\partial_t T - \frac{1}{\mathrm{RePr}} \frac{\kappa_s \rho_l c_{p,l}}{\kappa_l \rho_s c_{p,s}} \Delta T = 0 \qquad \text{in } \Omega_s(t), \tag{2.4}$$

with $\mathrm{D}(u) := \nabla u + (\nabla u)^T$, Re denoting the Reynolds number, Bo the Bond number, We the Weber number, Gr the Grashof number and Pr is the Prandtl number. The parameters $\kappa_{\{l,s\}}$, $\rho_{\{l,s\}}$ and $c_{p\{l,s\}}$ describe the heat conduction coefficient, the

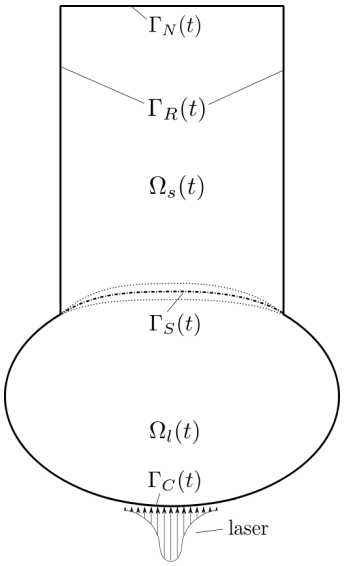

FIGURE 2.1. Sketch of geometry

density and the specific heat capacity in the liquid and solid phase. For the free capillary surface, the boundary conditions

$$u \cdot \nu = V_{\Gamma_C} \cdot \nu \qquad \text{on } \Gamma_C(t), \tag{2.5}$$

$$\sigma\nu = \frac{1}{\mathrm{We}} K\nu \qquad \text{on } \Gamma_C(t), \tag{2.6}$$

are prescribed. Thereby, V_{Γ_C} denotes the velocity of the free boundary, K is the sum of the principle curvatures and $\sigma := \frac{1}{\mathrm{Re}}\mathrm{D}(u) - p\mathrm{I_d}$ is the stress tensor. For the temperature, we impose

$$\frac{1}{\mathrm{RePr}}\partial_\nu T = \mathrm{La} I_l + \mathrm{Em}\left(T_a^4 - (T_m + T)^4\right) + \alpha\,(T_a - T) \qquad \text{on } \Gamma_C(t), \tag{2.7}$$

$$\frac{1}{\mathrm{RePr}}\frac{\kappa_s}{\kappa_l}\partial_n T = \mathrm{La} I_l + \mathrm{Em}\left(T_a^4 - (T_m + T)^4\right) + \alpha\,(T_a - T) \qquad \text{on } \Gamma_R(t), \tag{2.8}$$

$$\frac{1}{\mathrm{RePr}}\partial_\nu T = 0 \qquad \text{on } \Gamma_N(t). \tag{2.9}$$

to include laser heating, radiation and heat losses due to forced convection. Here, La is the laser number, Em is the emissivity and α is the scaled convective heat transfer coefficient. T_a denotes the ambient and T_m the melting temperature. In our model the temperature is scaled so that melting temperature corresponds to $T = 0$.

For handling the phase transitions during the process, we present shortly two different approaches which are combined for the numerical simulation.

2.2. **Enthalpy model.** The enthalpy model has been published in [13] and was further analyzed in [8]. In this paper, we adapt the model to a problem including thermal convection. The idea of the enthalpy model is to formulate the energy balance in the whole domain $\Omega(t)$ which is given by

$$\partial_t H + u\nabla H - \frac{1}{\mathrm{RePr}}\Delta T = 0 \quad \text{ in } \Omega(t), \tag{2.10}$$

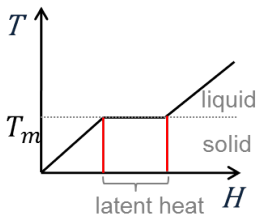

FIGURE 2.2. Temperature-enthalpy relation

with $u \equiv 0$ in $\Omega_s(t)$ and

$$T = \alpha(H) := \begin{cases} \frac{\rho_s c_{p_s}}{\rho_l c_{p_l}} H, & H < 0 \\ 0, & H \in \left[0, \frac{1}{\mathrm{Ste}}\right] \\ H - \frac{1}{\mathrm{Ste}}, & H \geq \frac{1}{\mathrm{Ste}} \end{cases} \tag{2.11}$$

describing the temperature-enthalpy relation where Ste denotes the Stefan number. Equation (2.11) is visualized in Figure 2.2. By solving equation (2.10), the solid-liquid interface $\Gamma_S(t) := \{x \in \Omega(t) | T(x) = 0\}$ is given implicitly. It is worth noting, that the enthalpy model can handle the nucleation and the vanishing of a liquid subdomain as well as multiple solid-liquid interfaces or a mushy region naturally.

2.3. **Sharp interface model.** Another model applicable for problems with phase transitions is a sharp interface model. Thereby, the solid-liquid interface $\Gamma_S(t)$ is defined as sharp boundary which is handled explicitly. On $\Gamma_S(t)$ the following boundary conditions are prescribed

$$u \cdot \nu = \left(1 - \frac{\rho_s}{\rho_l}\right) V_{\Gamma_S} \cdot \nu, \tag{2.12}$$

$$u - u \cdot \nu \, \nu = 0, \tag{2.13}$$

$$T = 0, \tag{2.14}$$

$$\frac{1}{\mathrm{RePr}} \left[(\nabla T)_l - \frac{\kappa_s \rho_l c_{p,l}}{\kappa_l \rho_s c_{p,s}} (\nabla T)_s \right] = \frac{1}{\mathrm{Ste}} V_{\Gamma_S}. \tag{2.15}$$

where $[\cdot]$ denotes the jump across the interface. The Stefan condition (2.15) reflects the thermal energy balance in the domain and is used to obtain the velocity V_{Γ_S} of the interface $\Gamma_S(t)$. A detailed description of the model can be found in [6].

3. NUMERICAL APPROACH

Numerical implementations of the enthalpy model and the sharp interface model have been integrated in the finite element solver NAVIER [4] to handle the phase transitions and to solve the PDE-system.

3.1. **Navier.** Originally, NAVIER has been developed for solving flow problems with free capillary surfaces, on time-dependent domains discretized by unstructured triangular grids. In NAVIER the Navier-Stokes equations are discretized by the Taylor-Hood element in space, i.e. piecewise quadratics for the velocities and piecewise linears for the pressure. For time discretization the fractional-step θ scheme in an operator splitting variant is applied [2]. The capillary surface is handled by using a semi-implicit, variational treatment of the curvature terms in the Navier-Stokes equations. Furthermore, the flow problem is decoupled from the geometry deformation in the fractional-step θ scheme.

3.2. **Enthalpy method.** The enthalpy FE method (basing on the enthalpy model) treats phase transitions implicitly. Consequently, the interface $\Gamma_S(t)$ is in general not given on element edges but intersects elements. To avoid the treatment of intersected elements in the flow problem, the following assumption is made: An element is considered to be liquid only, if the temperature at all of its nodes is equal or exceeds the melting temperature. Later, we will discuss the consequences of this simplification.

With this assumption, the numerical approach to solve the PDE-system given in Section 2 by applying the enthalpy model works the following way: Assume that approximations u^n, p^n of the fluid dynamics and of the temperature T^n are given on the actual geometry Ω^n for one time step n. To calculate the new domain Ω^{n+1} and the fluid dynamics u^{n+1}, p^{n+1} as well as the temperature T^{n+1} and H^{n+1} respectively, perform the three steps:

(1) Solve equation (2.10) in the actual domain Ω^n by using u^n for the convection term in the liquid subdomain to get the new temperature T^{n+1} and H^{n+1}.
(2) Update the domain's geometry $\Omega^{\tilde{n}}$ resulting from the new temperature T^{n+1} and define the new liquid subdomain $\Omega_l^{\tilde{n}}$ accordingly to the assumption above.
(3) Solve the fluid dynamics u^{n+1}, p^{n+1} on the new domain $\Omega_l^{\tilde{n}}$ by using the new temperature T^{n+1} resp. the new energy H^{n+1}, and update the geometry respectively to obtain Ω^{n+1}

Obviously, the temperature is solved before the fractional-step θ scheme is used for solving the fluid dynamics. Consequently, the new approximations u^{n+1}, p^{n+1} and T^{n+1} are calculated directly for the next time step.

3.3. **Sharp interface method.** In the numerical implementation of the sharp interface model, the domain is separated in a liquid and a solid subdomain by the interface $\Gamma_S(t)$ which is represented by edges of elements. On each subdomain the heat equation is solved independently using the interface as an internal Dirichlet condition. The jump of the temperature gradients across $\Gamma_S(t)$ is then used to derive its velocity, c.f. equation (2.15) .

At the same time, the deformation of the capillary surface is calculated by solving the Navier-Stokes equations. Finally, the whole outer geometry boundaries are moved accordingly to the deformation of the capillary surface $\Gamma_C(t)$ and the movement of the interface $\Gamma_S(t)$. By applying an ALE-approach, the interior mesh is moved as well, using an extension operator.

In short, the procedure for solving the PDE-system by applying the sharp interface method is as the following: Assuming that approximations u^n, p^n of the fluid dynamics and T^n of the temperature are given on the actual geometry Ω^n at time step n. To calculate the new domain $\Omega^{\tilde{n}}$ and the fluid dynamics $u^{\tilde{n}}$, $p^{\tilde{n}}$ as well as the temperature $T^{\tilde{n}}$ on it, perform the three steps

(1) Solve one step of the fractional-step θ scheme (Quasi-Stokes or Burger) to get an approximation $u^{\tilde{n}}$, $p^{\tilde{n}}$ of the fluid dynamics in the actual domain Ω^n.
(2) Derive the temperature $T^{\tilde{n}}$ on the domain Ω^n by treating $\Gamma_S^{\tilde{n}}$ as an internal Dirichlet boundary and using $u^{\tilde{n}}$ for the convection term of the heat equation.
(3) Obtain the boundary deformation by using the Stefan condition (2.15) and the kinematic boundary condition (2.5).

The the fluid flow u^{n+1}, pressure p^{n+1} and temperature T^{n+1} on the domain Ω^{n+1} are calculated after all steps of the fractional-step θ scheme have been performed.

Note that in contrast to the enthalpy method, the interdependence of interface and geometry is taken into account in every step of the fractional-step θ scheme.

Furthermore, it is important to note again that the sharp interface approach is an ALE-approach. Consequently, the phase boundary is a non-material surface, which means its movement is not influenced by the physical movement of material but the mesh and the material points are moved independently. A detailed description of the method is given in [6].

Remeshing and interpolation on new grid. Due to the evolution of the capillary surface in both methods and the mesh movement in the sharp interface approach, the mesh can degenerate during the simulation. Therefore, including a remeshing procedure and an interpolation method is mandatory for both approaches.

Remeshing. In our implementation, the software TRIANGLE [15] in combination with the adaptivity algorithms provided by NAVIER are used for mesh generation and remeshing. In more detail, the geometry boundary $\partial\Omega^n$ and the interface Γ_S^n are written as a planar straight line graph and then exported to TRIANGLE. Basing on given parameters describing e.g. the maximal edge length of elements, TRIANGLE creates a new mesh which is further adapted by NAVIER including a quadratic parametrization of the capillary surface Γ_C.

Interpolation. When creating a new mesh, the old data needs to be transferred onto the new grid. For this purpose, the interpolation algorithm presented in [1] is used. It is important to note that the interpolated velocity is no longer discretely divergence free on the new mesh. Consequently, the old velocity has to be projected directly onto the space of discretely divergence free functions on the new mesh via the L^2 inner product, c.f. [7].

3.4. **Comparing of both approaches.** Comparing the enthalpy method with the sharp interface approach, both methods show different pros and cons.

A advantage of the enthalpy method is its simplicity. Due to the transformation of the nonlinear effect of a moving interior boundary into the problem of treating the nonlinear temperature-enthalpy-relation, the numerics become straight forward. Moreover, this transformation results in a very good energy conservation in the solution while avoiding an explicit tracking of the moving interface $\Gamma_S(t)$ at the same time. An additional feature of the enthalpy method is the natural handling of nucleation and vanishing or mushy regions and multiple solid-liquid interfaces.

Unfortunately, a model for the flow in elements intersected by the interface $\Gamma_S(t)$ is needed in order to handle the fluid dynamics in the liquid subdomain. The simplification regarding the element's phase can lead to inaccuracy and numerical difficulties due to the coupling of the Stefan problem with the free capillary surface, especially, if sudden phase changes of elements at a curved capillary surface occur, c.f. Section 4. In addition, conservation of mass and momentum in this method is not straight forward.

The sharp interface method can simulate the melting process very exactly. The conservation of mass and momentum can be taken into account easily by conditions on the interior boundary. Furthermore, the method can handle the interdependence of triple junction and capillary surface very well which results in a very precise solution of the fluid dynamics.

A drawback of the sharp interface model is its incapability to handle topological changes. As a consequence, the solid and liquid subdomain have to exist from the very beginning. Moreover, the sharp interface approach is not able to handle the solidification process at all, due to the coupling of the triple junction and the

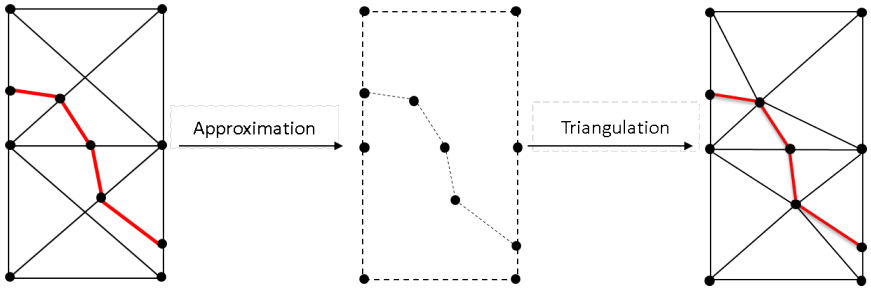

FIGURE 3.1. Generation of a new mesh including the interface Γ_S [12]

mesh movement and for the reasons mentioned above. Another disadvantage of the method is its complexity in regards to the numerical adaption.

3.5. **Combining both approaches.** By combining the enthalpy method and the sharp interface approach in the following way, we benefit from the advantages of both approaches and avoid the disadvantages at the same time:

We use the enthalpy method to simulate the nucleation of the liquid subdomain. After a few time steps when a sufficient liquid subdomain has been created, the method is switched and the sharp interface approach is applied. For this purpose, a sharp solid-liquid interface is defined as described in the section below and a new mesh including this explicit interface is generated.

Henceforth, the sharp interface method is used to simulate the melting process until the laser is switched off. When the solidification process begins, the geometry of the capillary surface is already evolved, we therefore can switch the method again using the enthalpy approach to simulate the liquid subdomain solidify without inaccuracy or numerical difficulties. This idea of coupling both approaches was first presented in [10].

Generation of Γ_S. To switch from the enthalpy method to the sharp interface approach, we need to generate a new mesh with element edges representing the interface Γ_S. Therefore, the approach presented in [12] is used: First, the interface Γ_S which is given implicitly in the enthalpy method is approximated by a polygonal line. This polygonal line and a planar straight line graph describing $\partial\Omega$ are then used by TRIANGLE for the generation of a new mesh. As before, we use the mesh algorithms of NAVIER afterwards for further mesh adaption and to represent the capillary surface Γ_C by a quadratic parametrization. The new generated mesh can now be moved accordingly to the algorithm given in Section 3.3.

4. RESULTS

In this section, we present some results of our finite element approach. Our application example is the laser-based free form heading process applied to a thin metallic wire. Due to the symmetry of this example, we use a 2D rotational symmetric approach.

4.1. **The combined finite element approach.** At first, the important steps of the combined finite element approach as described in the section above are visualized in Figure 4.1. Here, the solid subdomain is colored in light gray and and liquid subdomain is indicated in dark gray. Both domains are separated by the solid-liquid interface Γ_S.

By comparing the fluid flow simulated by using the enthalpy method with that obtained by using the combined approach, the benefit of the coupling becomes

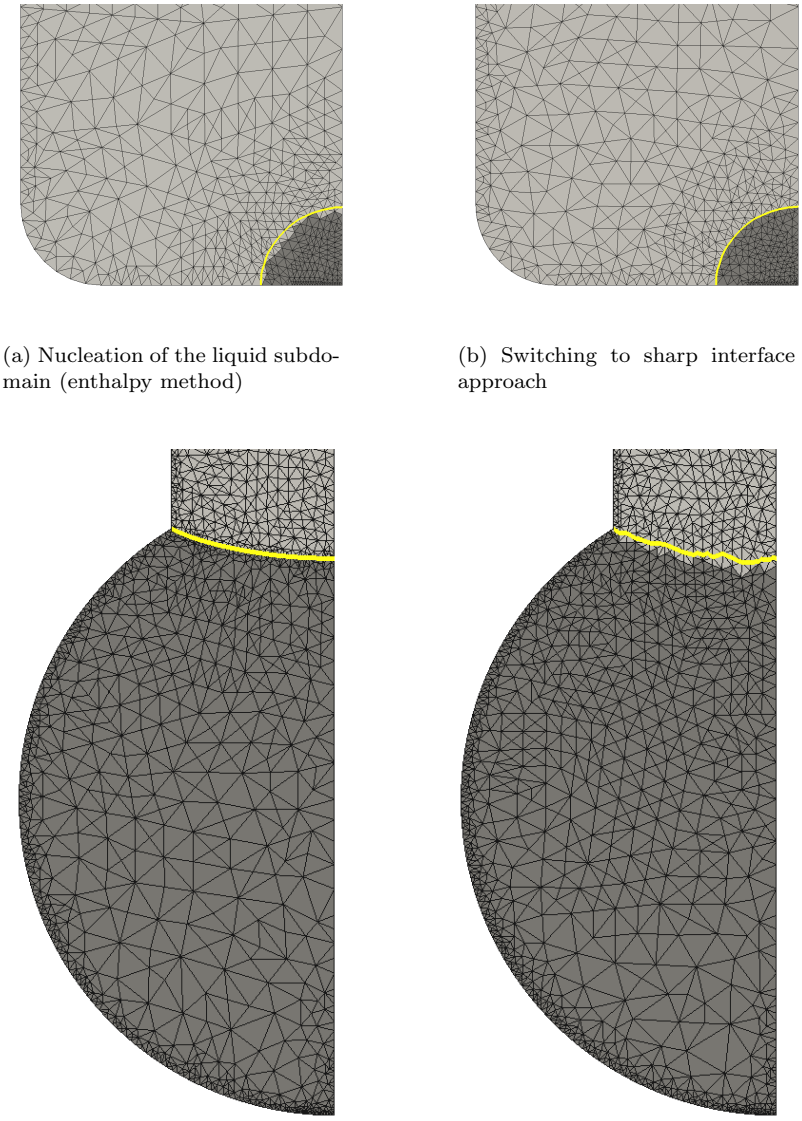

(a) Nucleation of the liquid subdomain (enthalpy method)

(b) Switching to sharp interface approach

(c) Sharp interface approach for simulation of the melting process

(d) Switching to enthalpy method for simulation of the solidification process

FIGURE 4.1. Visualization of combined finite element approach

obvious: If we use the enthalpy method for the simulation of the melting process, high oscillations in the fluid flow are dominating the flow field, see Figure 4.2(a). This is caused by the simplification of the liquid subdomain in the enthalpy method because as long as the solid-liquid interface move across an element, it is still treated as solid for the flow problem, see Figure 4.2(c).
Consequently, those elements can be considered as some kind of "barrier" for the flow which is suddenly removed if the melting temperature isoline has moved trough

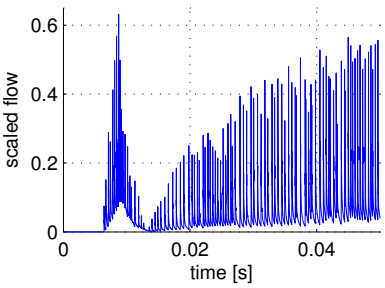

(a) Fluid flow for the first 50ms of the melting process simulated by the enthalpy method

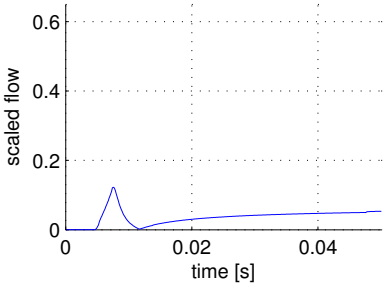

(b) Fluid flow for the first 50ms of the melting process simulated by the combined approach

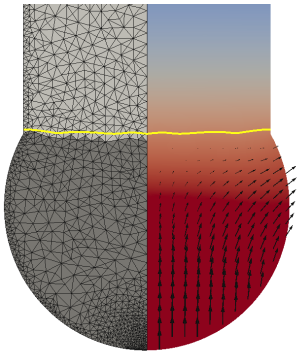

(c) Fluid flow in enthalpy method before an element at the capillary surface change its phase $t = 0.02963$ms

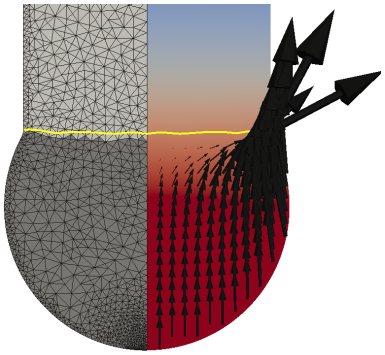

(d) Fluid flow in enthalpy method after an element at the capillary surface change its phase $t = 0.02964$ms

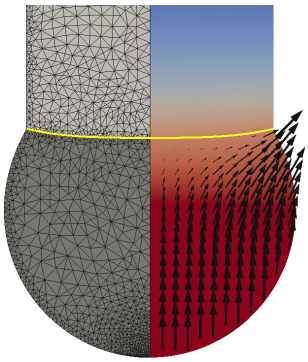

(e) Fluid flow in combined approach at $t = 0.02963$ms

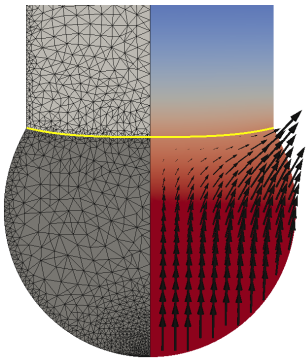

(f) Fluid flow in combined approach at $t = 0.02964$ms

FIGURE 4.2. Fluid dynamics in enthalpy method and in combined approach: (a) and (b) show the fluid flow velocity in both methods for the first 50ms of a melting process. A visualization of the flow in the simulation is given in Figure (c) -(f).

the whole element resulting in a very high and non-physical fluid flow, c.f. Figure 4.2(d), which can cause numerical difficulties.

By using the sharp interface approach for simulation the melting process, we avoid this problem and obtain realistic and very precise fluid flows 4.2(b) with no oscillations, c.f. 4.2(e) and 4.2(f) .

4.2. **Self-alignment.** Experiments performed by our cooperation partner BIAS revealed the laser-based free form heading to be self-aligning [3]. For our simulation, we show the consistency of the model and the finite element approach by using the same approach.

Similitude theory. In order to compare the experimental results for different rod diameters, a common approach is using the similitude theory of thermodynamics. By applying this theory to the given problem, the following scaling factors can be found [14]:

$$s_t = \left(\frac{d_{0,\text{new}}}{d_{0,\text{ref}}} \right)^2 \tag{4.1}$$

$$s_P = \left(\frac{d_{0,\text{new}}}{d_{0,\text{ref}}} \right)^{\frac{2}{3}} \tag{4.2}$$

Therefore, the irradiation time $t_{r,\text{new}}$ and the laser power $P_{L,\text{new}}$ for a sample with rod diameter $d_{0,\text{new}}$ can be obtained by

$$t_{r,\text{new}} = s_t t_{r,\text{ref}} \tag{4.3}$$

$$P_{L,\text{new}} = s_P P_{L,\text{ref}}. \tag{4.4}$$

By using this scaling factors in our application, we obtain the results shown in Figure 4.3 for wires with diameter $d_0 = 0.3\text{mm}$, $d_0 = 0.4\text{mm}$ and $d_0 = 0.5\text{mm}$. Thereby, we used different laser power denoted by P_{low} and P_{high} and different

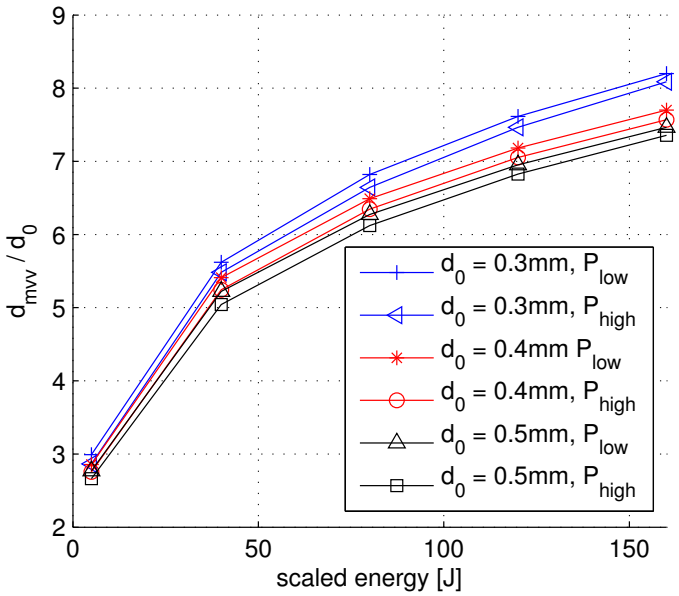

FIGURE 4.3. Results of self-alignment simulations for different rod diameters and energy pulses

irradiation times, respectively. All in all, the results show a good self-alignment property of the simulation and match the data presented in [3].

4.3. **Micro-structure.** A very important property for the forming process is the formability of the material accumulation. The formability of a specimen is primarily influenced by its micro-structure. Figure 4.4(a) shows a cross-section polish produced by the BIAS, in which the micro-structure is observable. The process parameters used in the experiment are given in the table 1.

Form the micro-structure we can deduce the course of the solidification process which can be compared to the simulation results, given in Figure 4.4(b) - 4.4(d). We notice that the simulation matches the experimental results very well. These results have been first presented in [9].

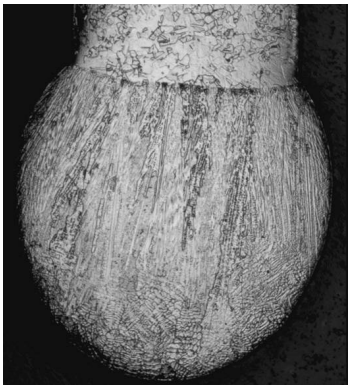

(a) Cross-section polish of specimen with rod diameter 0.5mm, process parameters are given in table 1

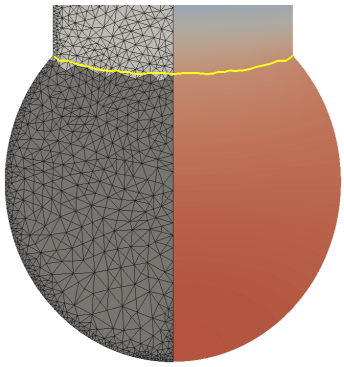

(b) Course of solidification isoline $t = 0.074$ms

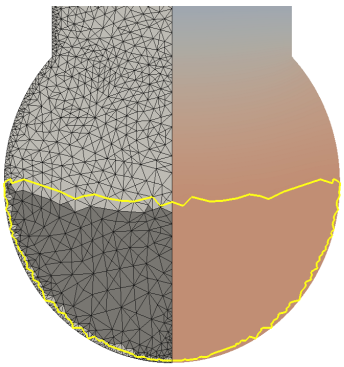

(c) Course of solidification isoline $t = 0.137$ms

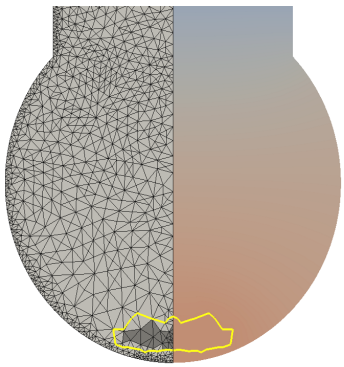

(d) Course of solidification isoline $t = 0.200$ms

FIGURE 4.4. Comparison of cross-section polish (a) with the course of the solidification isoline in the finite element simulation (b) - (d)

Laser type	Trumpf TruFiber 300
Power	80W
Pulse duration	50ms
Wire diameter	0.5mm
Shield gas	Nitrogen
Shield gas flow	$20\frac{\mathrm{l}}{\mathrm{min}}$

TABLE 1. Process parameter

5. Conclusions

A material accumulation process based on laser-based free form heading has been modeled by coupling the Stefan problem with the Navier-Stokes equations including a free capillary surface. For describing solid-liquid phase transitions, a enthalpy model and a sharp interface model have been presented. To benefit from their advantages, both models have been combined and were implemented in a finite element software, which has been used for the simulation of the melting and solidification process of a thin metallic wire. Furthermore, numerical results regarding the self-aligning behavior of the process and the solidification process have been presented.

Acknowledgement

The authors gratefully acknowledge the financial support by the DFG (German Research Foundation) for the subproject A3 within the Collaborative Research Center SFB 747 “Mikrokaltumformen - Prozesse, Charakterisierung, Optimierung”. Further, we want to thank the Bremer Institut für angewandte Strahltechnik (BIAS) and the AG Bänsch from the university of Nürnberg-Erlangen for cooperation.

References

[1] S. Basting. *A pdelib2 based Finite Element Implementation and its Application to the Mean Curvature Flow Equation*. Diplomarbeit, Universität Erlangen, 2009.

[2] M. O. Bristeau, R. Glowinski, and J. Periaux. Numerical methods for the Navier-Stokes equations. Application to the simulation of compressible and incompressible flows. *Computer Physics Report*, 6:73–188, 1987.

[3] H. Brüning and F. Vollertsen. Self-aligning capability of laser based free form heading process. In *Proceedings of 11th International Scientific Conference MMA - Advanced Production Technologies*, 2012.

[4] E. Bänsch. Finite element discretization of the Navier-Stokes equations with a free capillary surface. *Numerische Mathematik*, 88(2):203–235, 2001.

[5] E. Bänsch, J. Paul, and A. Schmidt. An ALE FEM for solid-liquid phase transitions with free melt surface. Technical Report 10-07, ZeTeM, Bremen, 2010.

[6] E. Bänsch, J. Paul, and A. Schmidt. An ALE finite element method for a coupled Stefan problem and Navier–Stokes equations with free capillary surface. *International Journal for Numerical Methods in Fluids*, 2012.

[7] E. Bänsch and A. Schmidt. Simulation of dendritic crystal growth with thermal convection. *Interfaces and Free Boundaries*, 2:95–115, 2000.

[8] C. M. Elliot. On the finite element approximation of an elliptic variational inequality arising from an implicit time discretization of the Stefan problem. *IMA Journal of Numerical analysis*, 1:115–125, 1981.

[9] M. Jahn, A. Luttmann, and A. Schmidt. A FEM simulation for solid-liquid-solid phase transitions during the production of micro-components. In *Proceedings of 11th International Scientific Conference MMA - Advanced Production Technologies*, 2012.

[10] M. Jahn, A. Luttmann, A. Schmidt, and J. Paul. Finite element methods for problems with solid-liquid-solid phase transitions and free melt surface. In *Proceedings in Applied Mathematics and Mechanics (PAMM)*, 2012. Accepted.

[11] T. Kokalj, J. Klemenčič, P. Mužič, I. Grabec, and E. Govekar. Analysis of the laser droplet formation process. *Journal of Manufacturing Science and Engineering*, 128(1):307–314, 2006.

[12] A. Kumar. From Isoline to Sharp Interface - Grid Generation. Technical report, ZeTeM, Bremen, 2010.

[13] L. I. Rubinšteĭn. *The Stefan Problem*, volume 27 of *Translations of Mathematical Monographs*. American Mathematical Society, Rhode Island, 1971.

[14] J. Sakkiettibutra and F. Vollertsen. Größeneffekte beim Stauchmechanismus am Beispiel geometrisch skalierter Brückenaktuatoren. *Größeneinflüsse bei Fertigungsprozessen*, pages 97–116, 2009.

[15] J. R. Shewchuk. Triangle: Engineering a 2d quality mesh generator and Delaunay triangulator. In *Selected papers from the Workshop on Applied Computational Geometry, Towards Geometric Engineering*, FCRC '96/WACG '96, pages 203–222, London, UK, UK, 1996. Springer-Verlag.

[16] A. Stephen and F. Vollertsen. Influence of the rod diameter on the upset ratio in laser-based free form heading. *Steel Research Int., Special Edition: 10th Int. Conf. on Technology of Plasticity (ICTP)*, pages 220–223, 2011.

[17] A. Visintin. *Models of phase transition*. Birkhäuser Boston Inc., 1996.

[18] F. Vollertsen. Categories of size effects. *Prod. Eng.-Res. Dev. 2*, pages 377–383, 2008.

[19] F. Vollertsen, D. Biermann, H.N. Hansen, I.S. Jawahir, and K. Kuzman. Size effects in manufacturing of metallic components. *CIRP Annals - Manufacturing Technology*, 58(2):566 – 587, 2009.

[20] F. Vollertsen and R. Walther. Energy balance in laser based free form heading. *CIRP Annals*, 57:291–294, 2008.

The Center for Industrial Mathematics, University of Bremen, 28359 Bremen
E-mail address: mischa@math.uni-bremen.de

The Center for Industrial Mathematics, University of Bremen, 28359 Bremen
E-mail address: schmidt@math.uni-bremen.de